International Journal of Applied Earth Observation and Geoinformation 28 (2014) 160–169

Contents lists available at ScienceDirect

International Journal of Applied Earth Observation and Geoinformation

journal homepage: www.elsevier.com/locate/jag

Estimation of real evapotranspiration and its variation in Mediterranean landscapes of central-southern Chile

L. Olivera-Guerra [a,*], C. Mattar [a], M. Galleguillos [b]

[a] Laboratory for Analysis of the Biosphere (LAB), University of Chile, Avenida Santa Rosa 11315, La Pintana, Santiago, Chile
[b] Department of Environmental Sciences, School of Agronomic Sciences, University of Chile, Avenida Santa Rosa 11315, La Pintana, Santiago, Chile

ARTICLE INFO

Article history:
Received 25 September 2013
Accepted 21 November 2013

Keywords:
Evapotranspiration
Rainfed landscape
S-SEBI
ASTER

ABSTRACT

Evapotranspiration (ET_d) is a key controller in the ecohydrological processes of semi-arid landscapes. This is the case of the dry land in Chile's central-southern zone, where forestry, farming and livestock activities must adapt to precipitation with considerable year-on-year variations. In this study, the spatial distribution of ET_d was estimated in relation to the land use map and physical parameters of the soil. The ET_d was estimated through the Simplified Surface Energy Balance Index (S-SEBI) using data from weather stations and remote data provided by the ASTER and MODIS sensors for November 2004 and 2006, respectively. The spatial variability of ET_d was compared among different plant types, soil textural classes and depths using non-parametric statistical tests. In this comparison, the highest rates of ET_d were obtained in the forest covers with values of 7.3 ± 0.8 and 8.4 ± 0.8 mm d^{-1} for 2004 and 2006, respectively. The lowest values were estimated for pastures and shrublands with values of 3.5 ± 1.2 mm d^{-1} and for crops with rates of 4.4 ± 1.6 mm d^{-1}. Comparison of the ET_d of the native forest covers and plantations of exotic species showed statistically significant differences; however, no great variation was noted, at least in the study months. Additionally, the highest rates of ET_d were found in the clay loam textures (6.0 ± 1.8 and 6.4 ± 2.0 mm d^{-1}) and the lowest rates in the sandy loam soils (3.7 ± 1.6 and 3.9 ± 1.6 mm d^{-1}) for 2004 and 2006, respectively. The results enable analysis of the spatial patterns of the landscape in terms of the relation between water consumption, ET and the biophysical characteristics of a Mediterranean ecosystem. These results form part of the creation of tools useful in the optimization of decision-making for the management and planning of water resources and soil use in territories with few measuring instruments.

1. Introduction

Evapotranspiration (ET_d) is a key component in the processes that guide the interactions of water and energy in semi-arid ecosystems. The water balance in these ecosystems is regulated by solar radiation and pluviometric events characterized by their low frequency and varied intensity, causing moisture in the soil that restricts soil-plant-atmosphere interactions. Under these conditions, ET_d represents a large proportion of the water budget, estimated at more than 70% of incoming precipitation (Kurc and Small, 2004; Huxman et al., 2005; Breshears, 2006; Moussa et al., 2007). In such landscapes, the soils store the incoming water from precipitation for potential biological activity (Huxman et al., 2004). This means that the variation in the availability of water resources is closely linked to changes in the physiological and structural states of the vegetation, which may be important in the control of ecological processes. Accordingly, ET_d is the central controller in ecohydrological processes in semi-arid environments, such as productivity of the ecosystem (Huxman et al., 2005; Yepez et al., 2005) and the influences of the vegetation on the water and the energy exchange (Moreira et al., 1996). Despite advances in the understanding of these phenomena, it has not yet been fully documented how the surface and subsurface characteristics of the soil can modify water and energy flows.

The Mediterranean landscape in Chile's central-southern zone is characterized by vast expanses of forest plantations and rainfed agricultural crops, mainly wheat, that must adapt to the rain cycles, which are scarce, intermittent and with significant year-on-year variations, as is frequently the case in semi-arid contexts (Newman et al., 2006). In addition to the water limitations during the dry season due to the absence of precipitation, water availability problems have intensified in recent decades. This is due to an increase in the demand for water for agricultural uses and human consumption (Lara et al., 2003), which may be critical in future

* Corresponding author. Tel.: +56 229785728.
E-mail address: luis.enrique.olivera@gmail.com (L. Olivera-Guerra).

0303-2434/$ – see front matter © 2013 Elsevier B.V. All rights reserved.
http://dx.doi.org/10.1016/j.jag.2013.11.012

scenarios given the climate change trends that project a decrease in precipitation and an increase in temperature in these territories (Fuenzalida et al., 2006).

Moreover, this zone has undergone strong man-made modifications, a product of the expansion of plantations of exotic forest species (mainly *Pinus radiata*), which has led to the elimination of extensive areas of native forest. This decrease has been estimated at 67% of the initial surface of native forest between 1975 and 2000 (Echeverria et al., 2006). These modifications in soil use and forest cover are important variables to consider in the hydrological cycle, and these have been studied regarding their effect on ET_d and water consumption (Bosch and Hewlett, 1982; Iroumé and Huber, 2002; Iroumé et al., 2006; Huber et al., 2008, 2010; Birkinshaw et al., 2011). Huber et al. (2008) reported greater water consumption (ET_d) on plantations of exotic species (*P. radiata* and *Eucalyptus* spp.) than on pasture and shrublands. These works focused mainly on catchment basins of less than 100 ha due to the greater control in the samplings, which increases their likelihood of success given that areas with fragmented landscape and reliefs could bias the results (Bosch and Hewlett, 1982). By contrast, in catchment basins of 100–1000 km^2, Pizarro et al. (2006) and Little et al. (2009) documented a decrease in the production of water flows due to the growth of forest plantation covers of exotic species to the detriment of the native forest.

Therefore, it is relevant to conduct studies on the spatial distribution patterns of ET_d and its relationship with various land use maps. Therefore, determining how ET_d is related to this information contributes to the understanding of processes that explain landscape hydrology, particularly on vast expanses and at a territorial level in the central-southern zone of Chile.

Surface energy balance models based on satellite images have successfully been applied to estimate the spatial distribution of ET_d in various landscapes. The Simplified–Surface Energy Balance Index (S-SEBI) (Roerink et al., 2000) is an algorithm that can estimate energy flows and ET_d through spatial contrasts between captured hydrological conditions and the information from satellite images regarding surface reflectance and the thermal region of the spectrum. This model requires a minimum of meteorological data, adapting to zones with few measurements in situ or that simply do not have these measurements. The S-SEBI model has been widely applied and evaluated successfully in obtaining the ET_d with different satellite sensors on an wide variety of ecosystems and at different spatial scales (Roerink et al., 2000; Gomez et al., 2005; Sobrino et al., 2005, 2007, 2008; Verstraeten et al., 2005; García et al., 2007, 2008; Boronina and Ramillien, 2008; Galleguillos et al., 2011; Mattar et al., 2013) on flat as well as mountainous terrains.

The spatial estimation of ET_d has been of interest to evaluate the characteristics of the landscape serving as an indicator of the water deficit of the surface (García et al., 2007, 2008), in the classification of functional types of ecosystems (Fernández et al., 2010), in the modeling of soil attributes (Taylor et al., 2013), and in the characterization of types of soil cover (Pôças et al., 2013).

Considering the aspects analyzed previously and the biophysical variables of the landscape that affect water consumption, the main objectives of this study focus on the dry landscape of the central-southern zone of Chile, (i) to evaluate the spatial distribution of ET_d in relation to the different land use maps and physical variables of the soil that determine the water storage capacity available for plants and (ii) to analyze the relevance of using ET_d to improve the understanding of spatial patterns throughout the territory.

The manuscript is structured as follows: Section 2 describes the study area, the data used and the methodology of this work. Section 3 presents the results and discussions on obtaining the spatial distribution of ET_d and its comparison with the biophysical variables associated with the vegetation and the physical properties of the soil. Finally, Section 4 presents the conclusions.

2. Data and methodology

2.1. Study area

The study area is two zones of the semi-arid sector of the Maule Region in central-southern Chile, located between 35°00′ and 35°50′ S, which cover a total area of 6050 km^2. This landscape has been drastically modified in recent decades due to a great expansion of plantations of exotic forest species (mainly of *P. radiata*), which led to the elimination of extensive areas of native forests (San Martín and Donoso, 1997), where Echeverria et al. (2006) estimated an annual reduction in native forest at a rate of 4.5%. The heavy development of forest activity has relegated the native forests to small patches (<100 ha) of secondary forests comprised mainly of *Nothofagus* (*N. obliqua* and *N. glauca*) and sclerophyll species such as *Acacia caven*, *Quillaja saponaria* and *Maytenus boaria* (Echeverria et al., 2006).

The area presents a Mediterranean climate with winter rains and a prolonged dry season between 7 and 8 months. Annual precipitation varies between 600 and 900 mm per year, concentrated mainly between May and August. The potential evaporation during the summer months is between 200 and 500 mm, exceeding the scarce rain. This zone is described by Little et al. (2009) as a semi-arid zone; however, according to the criteria of De Pauw et al. (2000) it is a sub-humid zone. In spite of this, the climatic conditions make the zone subject to a significant water deficit, which is critical in the dry season, with low cloud cover and high luminosity. These conditions enable the development of rainfed crops in the study area, mainly wheat, which must adapt to the scarce, intermittent rain cycles that vary considerably year-on-year.

To ascertain the topography of the terrain in the study area, a digital elevation model (DEM) was used via the ASTER GDEM, which has a spatial resolution of 30 m. This product was developed jointly by NASA and the Japanese Ministry of Economy, Trade and Industry (METI) and is freely available at http://www.gdem.aster.ersdac.or.jp/. The DEM was used to generate the slope and exposure maps needed to estimate solar radiation. In Fig. 1, an infrared composition appears on the DEM in the study area.

2.2. Spatial remote data and GIS

Two ASTER Level-2 product scenes were used of surface reflectance (AST-07), bands of surface emissivity (AST-5) and surface temperature (AST-08), which already have radiometric and atmospheric corrections (Abrams, 2000). The images of surface reflectance corresponding to the bands in the visible (Vis) and near infrared (NIR) were obtained at 15 m pixels, the bands in the shortwave infrared (SWIR) were obtained at 30 m pixels, while the products AST-5 and AST-8 corresponding to the bands in the thermal infrared (TIR) were obtained at 90 m pixels. The two scenes were acquired for November 5 2004 and November 18 2006 around 3 p.m. UTC (12 p.m. local time) under clear skies. The two scenes correspond to the period of maximum vegetation growth, where there are conditions of high radiation as well as optimal conditions in terms of water availability in the soil, this being immediately after the months where most of the rain is concentrated. Indeed, it has been shown in studies on Mediterranean ecosystems (Galleguillos et al., 2011) that during the spring-summer months the spatial differences of ET_d are maximized when there is a water deficit of varying magnitudes in the vegetation caused by the progressive exhaustion of the water reserves in soils. This phenomenon has greater impact on soils with physical properties that involve a lower retention capacity and subsequent delivery of water to the plants.

For the ASTER scenes, the Normalized Difference Vegetation Index (Rouse et al., 1973; Tucker, 1979) was calculated using the

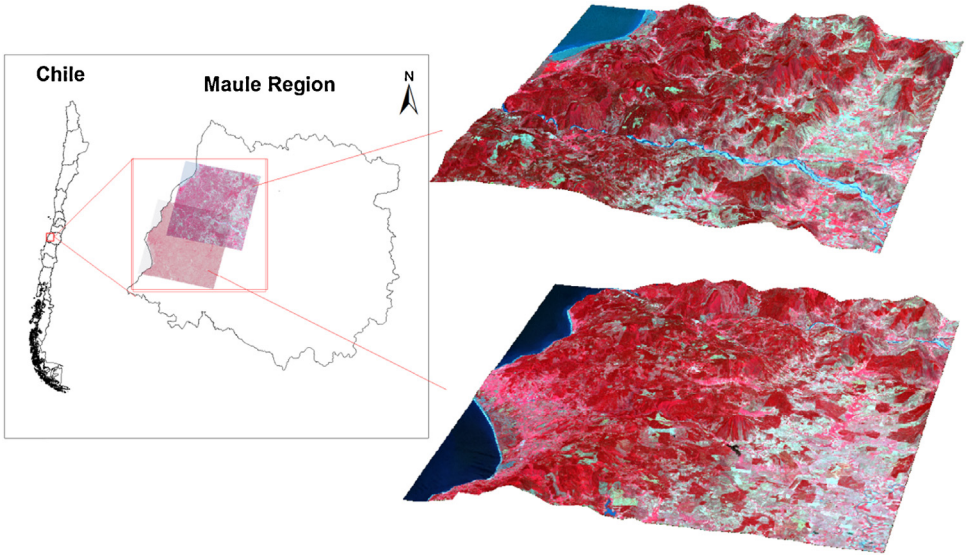

Fig. 1. Location of the study area. False color composition of the two ASTER scenes.

following ratio: the difference between the reflectance in the NIR and red wavelengths and the sum of these. Additionally, the air temperature at the moment the ASTER scenes passed over was obtained from the product MOD07 of the atmospheric profile, which provides air temperatures, among other variables such as surface pressure, with a spatial resolution of 5 km × 5 km at 20 pressure levels from 5 to 1000 hPa.

Orthorectified cartographic information was obtained from the Geographic Information Systems (GIS) from classes on land use maps and classification of soil types. Classes of landscape cover correspond to the Native Forest Registry for the Maule Region (Chile) updated in 2009 (Fig. 2). These were created through the interpretation of aerial photographs and satellite images at a scale of 1:50,000 using the Land Use Mapping (COT) developed by the Louis Emberger Center for Phytosociological and Ecological Studies (CEPE) in Montpellier, France, and adapted for Chile's ecological conditions by Etienne and Prado (1982). To obtain the physical properties of the soil analyzed in this work, GIS of the agrological study was used for the Maule Region (CIREN, 1997), presented in orthophotos at a scale of 1:20,000, which was created from agrological studies in the study area according to the technical standards of the Soil Survey Manual (Soil Survey Division Staff, 1993), and from which the classifications of textural classes and soil depths were obtained.

2.3. In situ data

The study area is not fully implemented in terms of meteorological data. Only daily minimum and maximum air temperature data were acquired, so two values per day are available to be processed. These data were collected from 10 stations of the agrometeorological network of the Chilean Meteorological Office, of which, according to the availability for the dates study, 8 stations were used for the 2004 scene and 6 for the 2006 scene. These data were used to obtain the global solar radiation at the time of acquisition from the satellite scenes. Also available was a series of weather data every 30 min of air temperature and solar radiation occurring at the Pantanillos station (35°28′ S, 72°18′′ W) for 2010 and 2011, with which the solar radiation estimation model was calibrated. In addition, the precipitation registered daily at the Constitución (35°19′ S, 72°24′ W) and Nirivilo (35°32′ S, 72°05′ W) stations, located in a common area for both scenes, were used. Table 1 summarizes the features of meteorological stations located over the study area.

2.4. Spatial estimation of meteorological data

The air temperature at surface level was obtained by interpolating the atmospheric profile (MOD07) in the first 1500 m of elevation (levels of pressure greater than 850 hPa) into the level of surface pressure, assuming a hydrostatic atmosphere, according to the equation:

$$T_a = (P_i - P_{surf})\frac{T_i - T_{850}}{P_i - 850} + T_i \quad (1)$$

where P_i is the level of pressure closest to the surface where data can be obtained (1000, 950 or 920 hPa), P_{Surf} is the surface pressure, T_i is the air temperature at the level of atmospheric pressure i, and T_{850} is the temperature at the 850 hPa level. The product obtained from the air temperature was resampled to a size of 90 m × 90 m pixels, using a regridding method based on cubic convolution, which consists of a non-linear interpolation as suggested by Zhao et al. (2005) for meteorological data.

The global solar radiation was obtained on the basis of the Bristow and Campbell (1984) model and described in detail in (Olivera et al., 2013). Although this model was defined for daily solar radiation values, it was evaluated successfully for monthly mean values (Meza and Varas, 2000), which is why this work used a new set of coefficients for an instantaneous time scale, calibrating the model for hourly data with the measurements from 2:30 p.m. and 3 p.m. (UTC) from the Pantanillos station for the clear days in November of 2010 and 2011. The model obtained a R^2 coefficient of 0.69 and a root mean square error (RMSE) of 48.7 W m^{-2} (5.1% relative error) in the calibration.

2.5. Estimation of daily evapotranspiration

To estimate evapotranspiration, the S-SEBI algorithm was used, which is an approach based on the balance of surface energy, which can be represented as follows:

$$\lambda ET_i = R_{ni} - G_{0i} - H_i \quad (2)$$

where R_{ni} is the net radiation resulting from the incident and outgoing shortwave and longwave radiation [W m^{-2}]; H is the sensible heat flow [W m^{-2}], G is the heat flow of the soil [W m^{-2}]; λET is the latent heat flow [W m^{-2}]; λ is the latent heat from vaporization of the water, approximately 2450 J g^{-1} at 20 °C; and ET represents the evapotranspiration [g m^{-2} s^{-1}]. The subindex 'i' refers to the

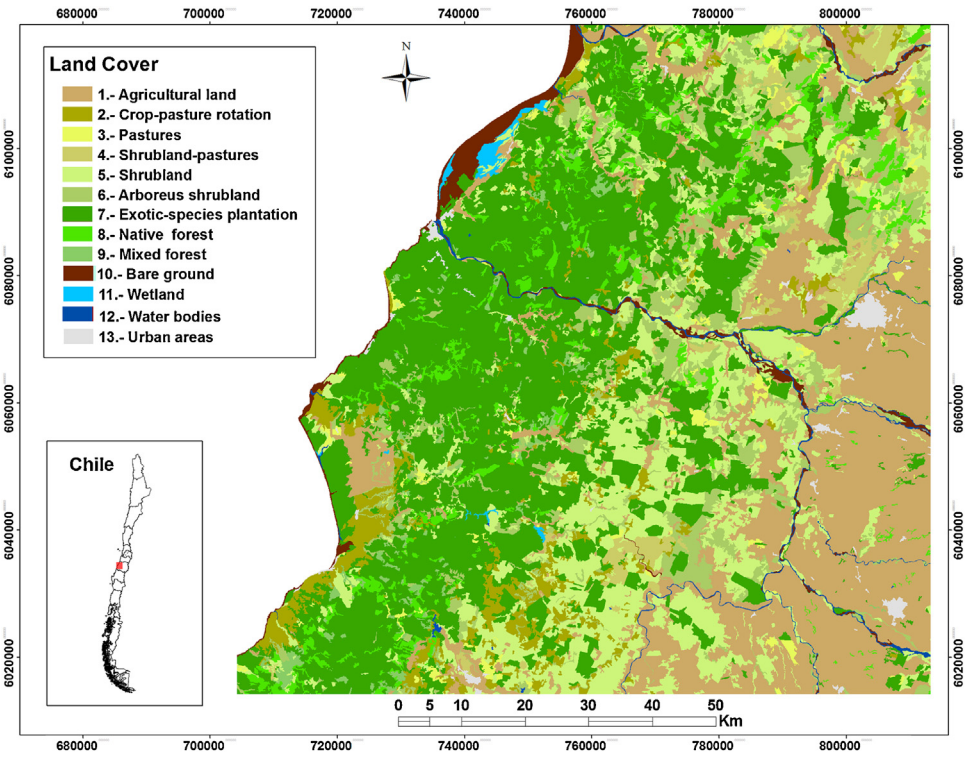

Fig. 2. Land use map of the study area.

instantaneous values whereas the subindex '*d*' is used for daily values.

To solve the components of Eq. (2), the S-SEBI model was used (Roerink et al., 2000) based on the surface contrasts that give account of the variability in hydrological conditions within the study area. These contrasts allow the theoretical limits, wet ($T_{\lambda ET}$) and dry (T_H), to be determined from a scatter plot of surface temperature values (T_s) and surface albedo (a_s) in order to derive the instantaneous *ET* pixel by pixel from the evaporative fraction (*EF*). This approach can be expanded to estimate daily evapotranspiration ET_d, which assumes $EF_i \cong EF_d$ and the negligible daily heat flow of the soil ($G_{0d} \cong 0$), whereas the net radiation at the moment the satellite passes (R_{ni}) can be extrapolated to a daily scale using the ratio $C_{di} = R_{nd}/R_{ni}$, which depends on the hour and day of the year (Sobrino et al., 2007). So ET_d can be expressed according to the following expression:

$$ET_d = 86400 \cdot EF_d \frac{R_{nd}}{\lambda} = 86400 \cdot \frac{T_H - T_s}{T_H - T_{\lambda ET}} \frac{(C_{di} R_{ni})}{\lambda} \quad (3)$$

The net radiation was derived from the ASTER and MODIS data using the general equation (Verstraeten et al., 2005; Chehbouni et al., 2008):

$$R_{ni} = (1 - a_s)R_g + \varepsilon_s(\sigma \varepsilon_a T_a^T - \sigma T_s^4) \quad (4)$$

where α_s is the surface albedo estimated according to Liang (2001) from the linear combination of the reflectance bands of the product AST-07 averaged to 90 m; R_g is the global solar radiation at the moment the satellite passes [W m^{-2}]; ε_s is the surface emissivity calculated from the emissivity bands of the product AST-05 (Ogawa et al., 2003); ε_a is the atmospheric emissivity [–], calculated from an empirical formulation in terms of the air temperature T_a (Bastiaanssen et al., 1998); σ is the Stefan–Boltzmann constant (5.67×10^{-8} [W m^{-2} K^{-4}]), and T_s is the surface temperature obtained directly from the product AST-08 [K].

Table 1
Meteorological data available for each weather station.

Weather station	Lat (°)	Long (°)	Altitude (m.a.s.l.)	2004	2006	2010–2011
Llico	34.45	72.07	10	*	*	
Curico	34.58	71.14	225		*	
Huaquen	35.06	71.42	150	*		
Panguilemo	35.22	71.28	113		*	
Talca	35.26	71.37	100	*	*	
San Pedro	35.28	72.24	553	*		
Dunas De Chanco	35.38	72.34	35	*		
Botacura	35.40	72.13	500	*		
Chanco	35.42	72.33	60	*	*	
Yerbas Buenas	35.45	71.34	150	*	*	
Pantanillos	35.47	71.30	312			***
Nirivilo	35.53	72.08	200	**	**	
Constitución	35.32	72.40	10	**	**	

* Daily minimum and maximum air temperature data (2 observations per day).
** Daily precipitation data for the whole year.
*** Air temperature, solar radiation and relative humidity each 30 min.

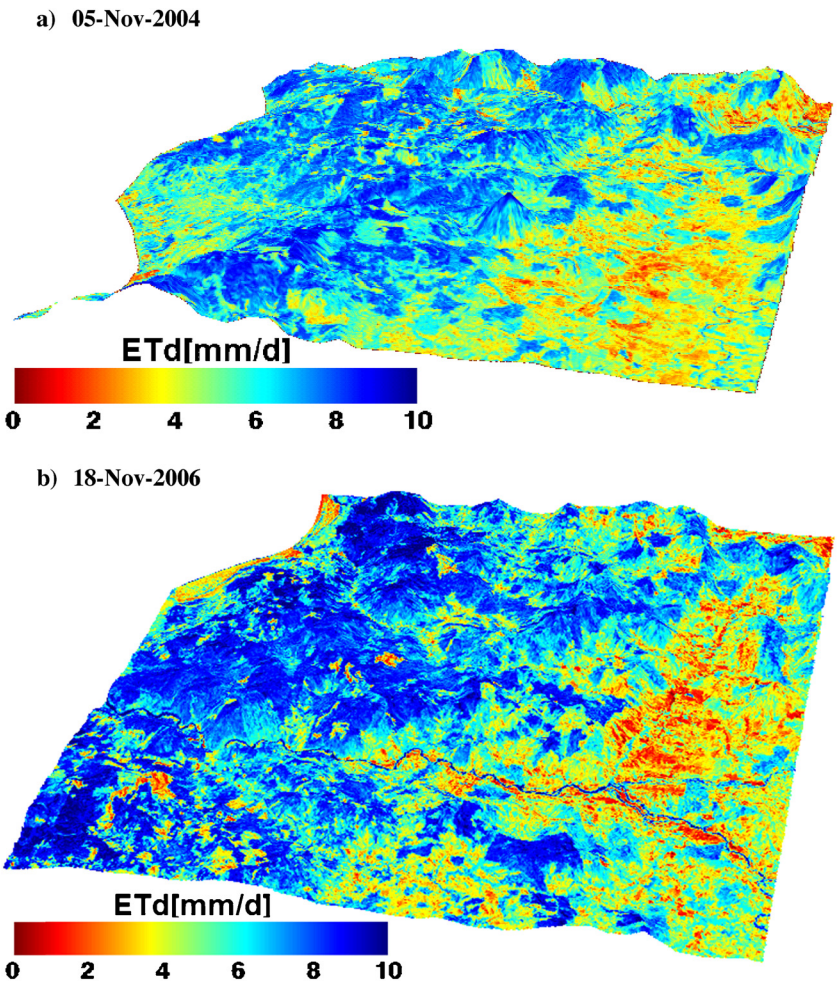

Fig. 3. Spatial distribution of ET_d for each scene.

2.6. Relationship between landscape and evapotranspiration

Once the ET_d was estimated from the balance of surface energy, it was compared to the biophysical variables of the land use map and physical properties of the soil: textural classes and depth.

The variation of the ET_d according to the variable landscape was analyzed from boxplots, for vegetation, soil texture and depth. For each variable, a sample was constituted from all the pixels that belonged to a class, so that for the ground cover 10 samples were compared, and for the properties of soil texture and depth, 5 samples for each were compared.

The spatial information was pre-processed, based on the elimination of zones where the relations were confused, such as those sectors that underwent strong degradation as a result of deforestation or logging, those that were visualized as bare soils or sectors with young vegetation. This filter made it possible to analyze in detail the ET_d patterns among the different forest covers.

In this comparison the behavior between classes of each variable of the landscape studied was analyzed, examining the significant differences existing between classes with the Kruskal–Wallis test of non-parametric contrasts and later by means of the Mann–Whitney non-parametric test to compare class with class. This study employed a 95% confidence level ($\alpha = 0.05$). To compensate for the Type I error due to the multiple comparisons in the Mann–Whitney contrast, the α level was divided by the number of comparisons according to each variable. It has to be noted that the statistical analysis was realized under the concept of areal model as described by Cressie (1991). This approach was chosen according to the ground data available which correspond to discrete data. Each polygon (or group of polygons) that represents a ground variable, gathering consequently thousands of pixels of ET_d, which were averaged for each class, diminishing significantly the probability of autocorrelation between ET_d and the classes.

3. Results and discussion

3.1. Daily evapotranspiration

Once the S-SEBI method had been applied to the two ASTER scenes, it was possible to obtain distribution maps of the ET_d on the dry land of the Maule Region (Fig. 3).

It is observed that in the 2006 scene higher rates were obtained than in that of 2004, so that in the 2004 scene the mean ET_d was 5.82 mm d^{-1} ($\pm$1.76) whereas in the 2006 scene the mean reached 6.39 mm d^{-1} ($\pm$2.08). This difference is due to meteorological input data, higher air temperature and global solar radiation, and can also be explained by a greater water availability due to the greater precipitation in 2006. Thus, the precipitation recorded in the period from April to the date of each image at the Constitución station was 751.0 and 929.3 mm for 2004 and 2006, respectively. In the same zone, the Nirivilo station presented values of 700.2 and 844.5 mm for the same years. This is why in 2006 the precipitation increased by 20.6% and 23.1% at both stations compared to 2004 (Fig. 4). This may reflect that there was a greater amount of water available in the soil, at least in the deepest layers, for the deep-rooted vegetation, and this will be discussed in further sections.

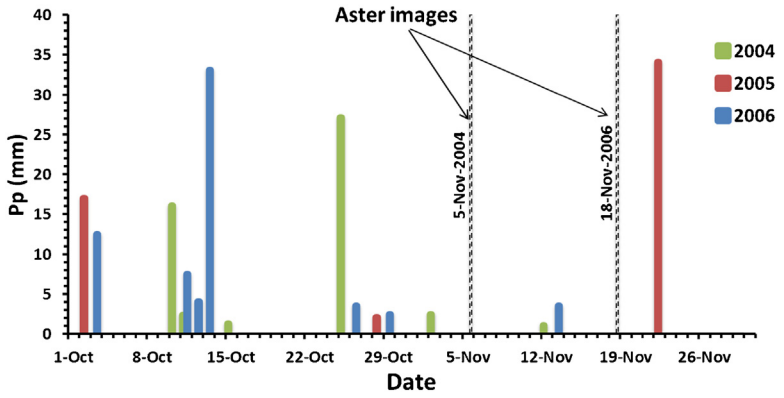

Fig. 4. Daily precipitation at the Nirivilo station for October and November between 2004 and 2006.

3.2. Relationship between daily evapotranspiration and vegetation

In a Fig. 5 box plot comparison is made for each scene between classes of the land use map, where practically the same trends can be observed between classes for both scenes.

In both scenes the highest ET_d rates (Figs. 3 and 4) were found in forest cover (Class 7–9), with means between 7.30 and 8.39 mm d^{-1}. This can best be seen in the comparison by box plot for the two scenes, in which the highest means appear (7.30–7.46 mm d^{-1} for the 2004 scene and 8.01–8.39 mm d^{-1} for the 2006 scene). Despite having very similar means, the classes show ET_d rates with statistically significant differences in both scenes, according to the Mann–Whitney non-parametric test, with the rates of forest plantations being higher than the native forests, and these in turn being higher than the mixed forests (Class 7 > Class 8 > Class 9). Similar studies have already shown these differences, where a greater water consumption by forest plantations, mainly of *P. radiata*, than by native forests has been determined (Huber et al., 2008; Lara et al., 2009; Little et al., 2009). In spite of the similarity in the results, in previous works these were obtained by estimating the water balance and water flow production. In this work equivalent results were established using remote sensing and spatially distributed energy balance estimation models.

The lowest rates of ET_d can be observed near the coast, in the southwestern zone of the 2004 scene and the northwestern zone of the 2006 scene, where there is terrain without vegetation (dunes), and in the interior of each scene (right), where rainfed agricultural activities, pastures and shrublands with less vegetation cover are developed. Fig. 4 illustrates the effect of vegetation on the amounts of ET_d such that the agricultural lands (Classes 1 and 2) present rates much lower than those obtained in forests, presenting similar means to meadowland, between 4.37 and 4.95 mm d^{-1} (Table 2). These low amounts of evapotranspiration in the crops correspond mainly to rainfed wheat. These crops are frequently found under conditions of water stress, mainly in the phenological stages after tasseling, corresponding to the dates of the satellite scenes where the plants are beginning the final maturation process with the resulting drying out of their plant structures. This significantly increases the sensible heat flow (and therefore the latent heat or ET_d decreases) when there is a low rate of structural humidity and physiological activity linked to canopy transpiration.

In terms of shrub-pasture, shrubland and arboreous shrubland covers (Classes 4–6), these show an increase in ET_d due to the increase in shrub and tree cover. This may be due to the water contained in the upper layers of soil beginning to dry up on these dates, which is why shrubs and trees have more water available in the deeper layers. Zhang et al. (2001) and Huxman et al. (2005) have determined that the invasion of ligneous plants into ecosystems changes the components of the hydrological cycle, reducing the flows generated and increasing the transpiration of the vegetation when using the water available in the soil. At the same time, they suggest that these changes are more relevant in semi-arid ecosystems, being small or negligible in arid and sub-humid

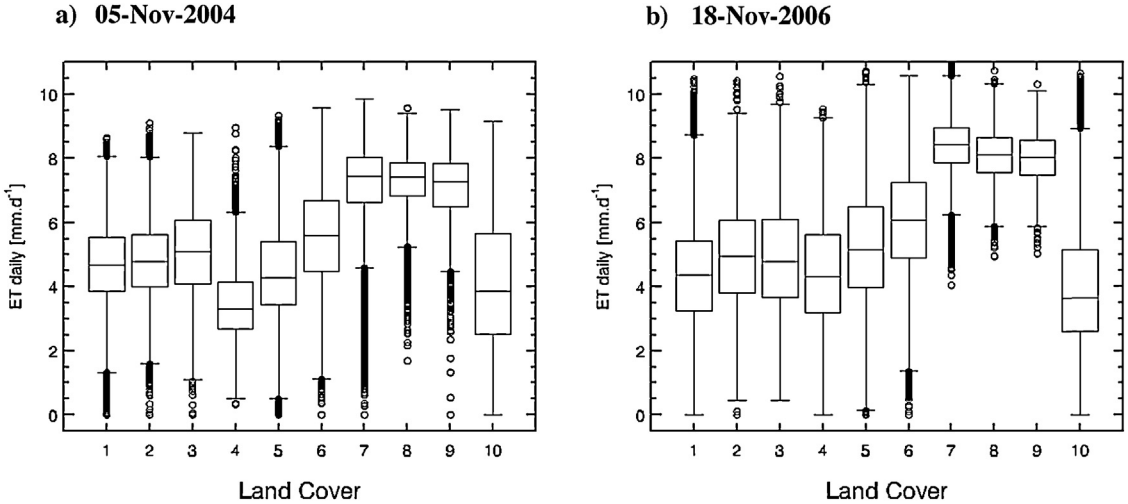

Fig. 5. Box plot of ET_d per class of soil use for each scene. 1: agricultural land; 2: crop-pasture rotation; 3: pastures; 4: shrubland-pastures; 5: shrubland; 6: arboreus shrubland; 7: exotic-species plantation; 8: native forest; 9: mixed forest; 10: bare ground.

Table 2
Descriptive statistics of ET for each satellite date and land cover type.

Land cover	Mean		Std. Dev.		*n*	
	2004	2006	2004	2006	2004	2006
AL	4.67	4.37	1.27	1.61	25,492	40,971
CPR	4.84	4.95	1.19	1.67	31,423	6,884
Pas	5.04	4.94	1.47	1.76	4,577	5,956
SP	3.46	4.48	1.15	1.78	7,718	9,471
Shr	4.50	5.26	1.43	1.79	80,351	59,188
AS	5.55	6.03	1.48	1.61	34,590	42,163
ESP	7.46	8.39	0.88	0.82	140,313	76,894
NF	7.39	8.10	0.75	0.80	13,057	11,109
MF	7.30	8.01	0.86	0.81	4,587	1,714
BG	4.18	4.03	2.10	2.01	3,379	6,197
Average	5.82	6.39	1.76	2.08	345,487	260,547

StdDev: standard deviation; N: number of pixels included in each land cover type; AL: agricultural land; CPR: crop-pasture rotation; Pas: pastures; SP: shrubland-pastures; Shr: shrubland; AS: arboreus shrubland; ESP: exotic-species plantation; NF: native forest; MF: mixed forest; BG: bare ground.

environments. This is reflected in the study area, where the forest plantations present the greatest evapotranspiration rate compared to the rest of the surface covers. With different methods and for the same study area, similar results were reported by (Huber et al., 2008), where similar differences were found between plantations of *P. radiata* compared with pastures and shrubs, also demonstrating a reduced percolation and high water consumption due to evapotranspiration.

To determine the influence of vegetation on ET_d rates quantitatively, the NDVI spectral vegetation index was compared with the ET_d through a scatter diagram (not shown), obtaining a linear regression with a high correlation (R^2 of 0.76 and 0.78 for the 2004 and 2006 scenes, respectively). Therefore, the NDVI might explain in large measure the ET_d recorded in the zone, as has been demonstrated in works on various ecosystems (Yang et al., 2006; Cleugh et al., 2007; Mu et al., 2007; Wang et al., 2007; Glenn et al., 2008). Additionally, the NDVI is an easy variable to obtain through remote sensing, having the advantage that surface reflectance is a greater spatial resolution than thermal images required in the estimation of energy flows.

With respect to the areas without vegetation (Class 10), the great variability recorded stands out, where the quartiles are distributed practically between the minimum and maximum amounts of ET_d found in each scene. This situation is explained basically by the presence of vegetation, bodies of water and wetlands formed in the middle of the dunes in both scenes, classified according to the GIS as cover within Class 10. This occurs because the minimum mapping area of 6.25 has, where dunes coexist, is composed of dry zones with minimum ET_d rates, both as wetlands and bodies of water, the ET_d rates of which are the maximum.

According to the test of contrasts between classes, the Mann–Whitney test revealed that the only classes that did not show any significant differences in their measures of central tendency were the crop-pasture rotation and pasture, croplands and shrubland-pasture in the 2006 scene. These results pointed out the logical response in water consumption between vegetation that has ecological similarities in terms of structural and functional properties such as architecture, height of individual, depth rooting and fenological periods that depends mainly on rainy season. In this case, the last precipitation event was registered 36 days before the satellite overpass (Fig. 4), even though that in 2006 the total precipitations were higher than in 2004. Therefore the soil surface was probably dried enough to undifferentiated the effect of water consumption, expressed as ET_d, between all types of vegetation classes that interact with available water stored in the soil. It may represent one of the uncertainties of the proposed approach.

Meanwhile, in the 2004 scene all the results between classes showed statistically significant differences. These results highlight the relevance of ET_d as an ecosystem functional tool (García et al., 2008; Fernández et al., 2010), able to discriminate among all the land use classes. In this condition, where a 28 mm rain was registered 11 days before the ASTER scene, soil moisture was enough to allow transpiration of non-stressed plants, highlighting the physiological and structural capacities of the vegetation to produce different ET_d rates.

3.3. Relationship between daily evapotranspiration and physical properties of the soil

Figs. 6 and 7 illustrate the comparison using boxplots for each scene between textural classes and soil depth, respectively. In terms of the ET_d patterns according to textural classes, with the exception of the sandy textures, confirms the theoretical trend of the relationship between textures and the water exchange capacity, recording very similar patterns between classes in both scenes. The highest ET_d rates were found in the clay loam textures with means of 6.04 (±1.76) and 6.40 (±1.97) mm d^{-1} and the lowest rates in the sandy loam soils with means of 3.72 (±1.57) and 3.95 (±1.59) mm d^{-1} for the 2004 and 2006 scenes, respectively.

This tendency between classes is explained basically by the different capacity that the soils have in delivering available water to the vegetation and which is conditioned in part by this physical attribute. Thus, the finest textures presented greater surface per unit of volume, enabling a greater adsorption of water films by soil particles. Nevertheless, it is precisely due to this phenomenon that the water is heavily retained in the soil, limiting absorption by the roots, which leads to the resulting decrease in the plant transpiration rate. It is for this reason that loam textural classes are those with the greatest water availability for the plants, since they present the greatest amount of micro and macropores, and the coarse textural classes (sand and sandy loam) present the lowest quantity of available water. However, the sandy class did not exhibit the expected tendency, registering elevated ET_d rates, which might be associated with factor related to vegetation, bodies of water and small wetlands and meadows that can be found in the middle of the sand dunes, as previously mentioned for the cover of areas without vegetation. A comparison of the coarse classes in both scenes revealed that the 2004 scene presented higher ET_d rates, since attempts have been made to control the movements of sand through the extensive plantation of marram grass (*Ammophila arenaria*) (Castro, 1988), as well as the construction of the Federico Albert National Reserve. This reserve contains forest species (*Eucaliptus globulus*, *P. radiata*, *Cupressus macrocarpa*, *Acacia melanoxylon*) introduced to control the expansion of the dunes on the town of Chanco (Paskoff and Manriquez, 1999). This is why this

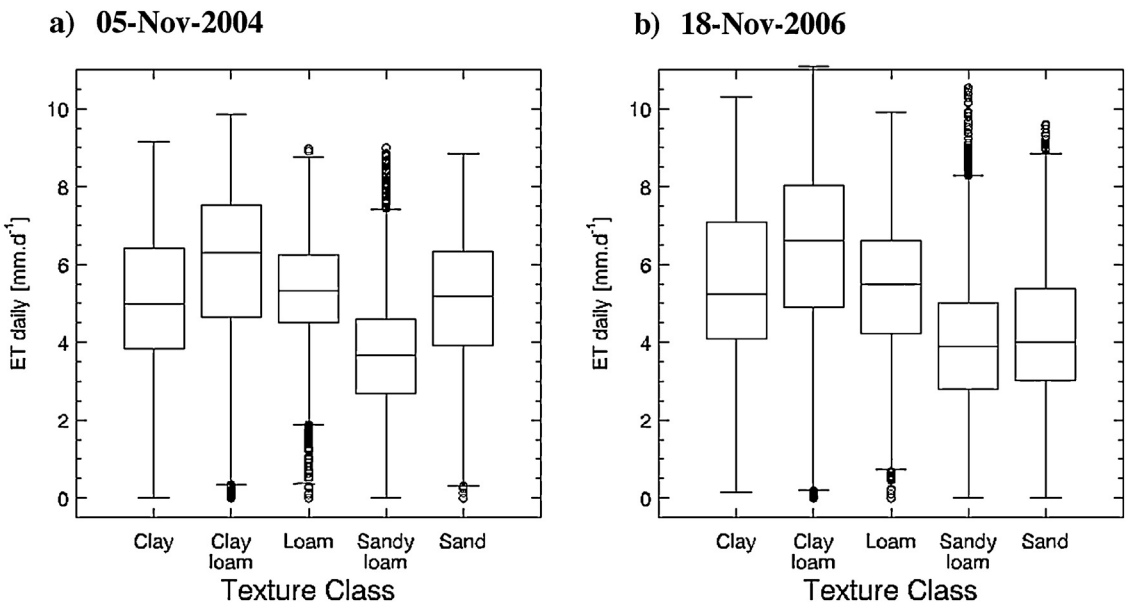

Fig. 6. Box plot of ET_d per class of texture of the soil for each scene.

textural class presents a greater ET_d due to the NDVI increase over the sand cover.

Similar tendencies were found in both scenes (2004 and 2006) in the ET_d by textural class. Previous studies have focused on determining the effect of soil textures on the water properties of those soils, defining the relationship between soil moisture, load and hydraulic conductivity (Fernandez-Illescas et al., 2001; Gutmann and Small, 2005; El Maayar and Chen, 2006). Thus, this movement controls the water balance between evapotranspiration and runoff. Despite these relationships between texture and ET_d, Gutmann and Small (2005) showed that the textural classes alone explain between 4% and 14% of the energy flows used in *ET*.

In box plots by soil depth class (Fig. 7), the ET_d did not present the same patterns between classes in the two scenes; the greatest differences were found between scenes in the thinnest soils. Nevertheless, in both scenes it was observed that the thinnest soils (<75 cm) exhibited the lowest rates of ET_d, the minimum being in the soils between 25 and 50 cm with rates of 3.84 (±1.24) and 4.13 (±1.53) mm d^{-1} for the 2004 and 2006 scenes, respectively. The soils between 75 and 100 cm had the highest evapotranspiration rates, with means of 6.45 (±1.55) and 7.11 (±1.77) mm d^{-1} for the 2004 and 2006 scenes. This is due mainly to the greater water storage capacity of deep soils due to the greater volume per ground surface. The deepest soils (>100 cm), however, did not present the highest rates, being exceeded by those previously mentioned. This can be explained by the type of vegetation developed in each depth class, since, as can be seen in Table 3, the soils between 75 and 100 cm are covered mainly by forests (996.5 and 651.7 km^2) whereas >100 cm have a large proportion of surface covered by agricultural crops and pastures and shrublands (456.2 and 638.6 km^2). These deeper soils presented vegetation with short phenological cycles, strongly dependent on surface water; therefore, for the

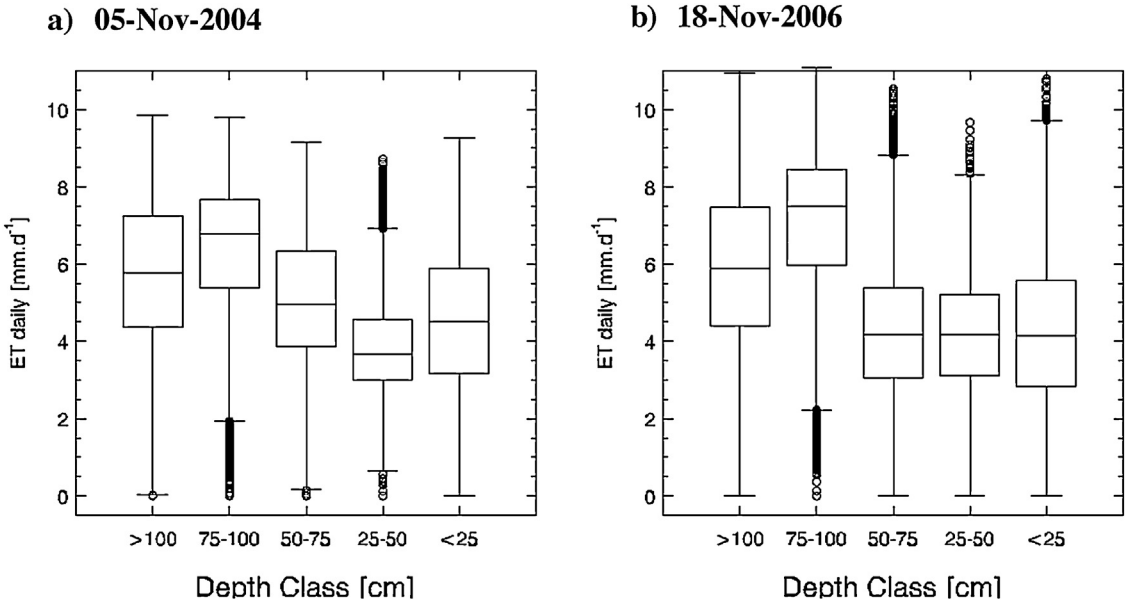

Fig. 7. Box plot of ET_d per class of soil depth for each scene.

Table 3
Surface of the main land cover type for each satellite date and depth class.

Land cover type	Date	Depth class [cm]					
		>100	75–100	50–75	25–50	<25	Total
Agricultural land (AL, CPR)	2004	238.7	73.8	103.7	21.0	4.1	441.4
	2006	225.4	44.2	61.9	26.9	17.4	375.8
Pastures and shrubland (Pas, SP, Shr, AS)	2004	456.2	248.8	165.6	127.0	14.3	1011.9
	2006	638.6	239.9	28.3	7.6	15.6	930.1
Forests (ESP, NF, MF)	2004	831.6	996.5	150.8	19.4	2.4	2000.7
	2006	613.5	651.7	14.5	1.3	5.0	1286.0
Total	2004	1526.6	1319.2	420.0	167.4	20.8	3454.1
	2006	1477.5	935.8	104.7	35.8	38.0	2591.9

Note: The satelite scenes correspond to spatially different areas, which is why the surface of the classes is.

study dates the transpiration rate was much lower than in sectors with forests and soils that were not as deep. These results are consistent with what was reported by Echeverria et al. (2007), who compared the water consumption of a pasture and a native forest in southern Chile. In this study the marked seasonal fluctuation of the moisture content in the soil was verified, with the pasture being the one that presented the most intense drying patterns in the first 100 cm of depth.

The two scenes had dissimilar trends for the ET_d based on the soil depth as illustrated in Fig. 7. Here it can be seen that for the 2006 scene, the three thinnest soil classes (classes < 75 cm) did not present significant differences in their rates, as were found in the 2004 scene. This can be explained in part by the type of vegetation developed and the pluviometric events recorded before each date of analysis. This way, for the 2006 analysis date no significant precipitation was recorded on the previous days (3.5 mm) (Fig. 4), with the last relevant rain being one month prior to the acquisition date. This resulted in significant drying of thin soils (classes < 75 cm), causing low evapotranspiration rates at the time of the scene. By contrast, for the 2004 scene, significant differences were found in the ET_d between all the classes, including those of surface soils, when conditioned by the significant precipitation (29.6 mm) recorded ten days before the acquisition of the scene (Fig. 4). This may indicate that there was sufficient water available in the thinnest soils, which is why the differences between classes might be due to the water consumption by the type of vegetation present.

4. Conclusions

The use of the S-SEBI model permitted estimation of ET_d on a regional scale in the dry land of Chile's central-southern zone, which does not have adequate instrumentation to monitor water and energy flows. The model was fed with ASTER images with a high spatial resolution, which was complemented with information from the MODIS sensor and meteorological data in situ of daily maximum and minimum temperatures.

The proposed methodology enabled comparison of the differences between the land use maps and soil types that compose the landscape of the zone, contributing important information regarding water consumption in the territory. Thus, the highest ET_d rates were obtained in the forest covers with values of 7.3 ± 0.8 and 8.4 ± 0.8 mm d^{-1} for 2004 and 2006, respectively. The plantations of exotic species had slightly higher rates than the native forests, and their differences were statistically significant. As far as the physical properties of the soil are concerned, it was established that the textural classes and depth are associated with ET_d following the theoretical patterns associated with water availability in the soil for the plants. It should be pointed out that the time distribution of the pluviometric events and the type of soil dependent on the vegetation cover developed in it were factors of interest to explain the spatial patterns of the ET_d.

These results improve understanding of the spatial patterns of the landscape based on quantitative results regarding the relationship that exists with the water consumption evaluated as ET and the biophysical characteristics of the study zone. This work sets a precedent in the generation of tools to optimize decision-making in the management and planning of water resources in territories of dry land with insufficient measuring instruments, supporting future integrated strategies for dealing with water and soil use. It is worth emphasizing that the results become increasingly relevant because of this being a zone declared as susceptible to climate change, and there are currently problems of water availability, which makes the search for solutions for future adverse scenarios all the more acute.

Acknowledgements

This work was partially funded by Program U-INICIA VID 2012, grant U-INICIA 4/0612; University of Chile and the CONICYT project, Integration of Advanced Human Capital into the Academy, code 791100013. The authors also thank to the MODIS team for provided atmospheric products (http://modis-atmos.gsfc.nasa.gov/).

References

Abrams, M., 2000. International Journal of The Advanced Spaceborne Thermal Emission and Reflection Radiometer (ASTER): data products for the high spatial resolution imager on NASA's Terra platform. Int. J. Remote Sens. 21, 847–859.
Bastiaanssen, W.G.M., Menenti, M., Feddes, R.A., Holtslag, A.A.M., 1998. A remote sensing surface energy balance algorithm for land (SEBAL). 1. Formulation. J. Hydrol. 212–213, 198–212.
Birkinshaw, S.J., Bathurst, J.C., Iroumé, A., Palacios, H., 2011. The effect of forest cover on peak flow and sediment discharge – an integrated field and modelling study in central-southern Chile. Hydrol. Process 25, 1284–1297.
Boronina, A., Ramillien, G., 2008. Application of AVHRR imagery and GRACE measurements for calculation of actual evapotranspiration over the Quaternary aquifer (Lake Chad basin) and validation of groundwater models. J. Hydrol. 348, 98–109.
Bosch, J.M., Hewlett, J.D., 1982. A review of catchment experiments to determine the effect of vegetation changes on water yield and evapotranspiration. J. Hydrol. 55, 3–23.
Breshears, D.D., 2006. The grassland-forest continuum: trends in ecosystem properties for woody plant mosaics? Front. Ecol. Environ. 4, 96–104.
Bristow, K., Campbell, G., 1984. On the relationship between incoming solar radiation and daily maximum and minimum temperature. Agric. For. Meteorol. 31, 159–166.
Castro, C.A., 1988. The artificial construction of foredunes and the interference of dune-beach interaction, Chile. J. Coast. Res. Spec. Issue 3, 103–109.
Chehbouni, A., Hoedjes, J.C.B., Rodriquez, J., Watts, C.J., Garatuza, J., Jacob, F., Kerr, Y.H., 2008. Using remotely sensed data to estimate area-averaged daily surface fluxes over a semi-arid mixed agricultural land. Agric. For. Meteorol. 148, 330–342.
CIREN, 1997. Estudio Agrológico VII Región. Descripciones de Suelos. Materiales y Símbolos, Santiago, Chile, pp. 611.
Cleugh, H.A., Leuning, R., Mu, Q., Running, S.W., 2007. Regional evaporation estimates from flux tower and MODIS satellite data. Remote Sens. Environ. 106, 285–304.
Cressie, N.A.C., 1991. Statistics for Spatial Data. Wiley, New York.

De Pauw, E., Göbel, W., Adam, H., 2000. Agrometeorological aspects of agriculture and forestry in the arid zones. Agric. For. Meteorol. 103, 43–58.
Echeverria, C., Coomes, D., Salas, J., Rey-Benayas, J.M., Lara, A., Newton, A., 2006. Rapid deforestation and fragmentation of Chilean temperate forests. Biol. Conserv. 130, 481–494.
Echeverria, C., Huber, A., Taberlet, F., 2007. Estudio comparativo de los componentes del balance hídrico en un bosque de nativo y una pradera en el sur de Chile. Bosque 28 (3), 271–280.
El Maayar, M., Chen, J.M., 2006. Spatial scaling of evapotranspiration as affected by heterogeneities in vegetation, topography, and soil texture. Remote Sens. Environ. 102, 33–51.
Etienne, M., Prado, C., 1982. Descripción de la vegetación mediante la Cartografía de Ocupación de Tierras. Conceptos y manual de uso práctico. Universidad de Chile. Facultad de Ciencias agrarias, veterinarias y forestales, Departamento de producción animal, Santiago, pp. 120.
Fernández, N., Paruelo, J.M., Delibes, M., 2010. Ecosystem functioning of protected and altered Mediterranean environments: a remote sensing classification in Doñana, Spain. Remote Sens. Environ. 114, 211–220.
Fernandez-Illescas, C.P., Porporato, A., Laio, F., Rodriguez-Iturbe, I., 2001. The ecohydrological role of soil texture in a water-limited ecosystem. Water Resour. Res. 37, 2863–2872.
Fuenzalida, H., Aceituno, P., Falvey, M., Garreaud, R., Rojas, M., Sanchez, R., 2006. Study on climate variability for Chile during the 21st century. Technical Report prepared for the National Environmental Commission CONAMA, Santiago, Chile.
Galleguillos, M., Jacob, F., Prévot, L., French, A., Lagacherie, P., 2011. Comparison of two temperature differencing methods to estimate daily evapotranspiration over a Mediterranean vineyard watershed from ASTER data. Remote Sens. Environ. 115, 1326–1340.
García, M., Oyonarte, C., Villagarcía, L., Contreras, S., Domingo, F., Puigdefábregas, J., 2008. Monitoring land degradation risk using ASTER data: the non-evaporative fraction as an indicator of ecosystem function. Remote Sens. Environ. 112, 3720–3736.
García, M., Villagarcía, L., Contreras, S., Domingo, F., Puigdefábregas, J., 2007. Comparison of three operative models for estimating the surface water deficit using ASTER reflective and thermal data. Sensors 7, 860–883.
Glenn, E.P., Huete, A.R., Nagler, P.L., Nelson, S.G., 2008. Relationship between remotely-sensed vegetation indices, canopy attributes, and plant physiological processes: what vegetation indices can and cannot tell us about the landscape. Sensors 8, 2136–2160.
Gomez, M., Olioso, A., Sobrino, J., Jacob, F., 2005. Retrieval of evapotranspiration over the Alpilles/ReSeDA experimental site using airborne POLDER sensor and a thermal camera. Remote Sens. Environ. 96, 399–408.
Gutmann, E.D., Small, E.E., 2005. The effect of soil hydraulic properties vs. soil texture in land surface models. Geophys. Res. Lett. 32, L02402.
Huber, A., Iroumé, A., Bathurst, J.C., 2008. Effect of *Pinus radiata* plantations on water balance in Chile. Hydrol. Process. 148, 142–148.
Huber, A., Iroumé, A., Mohr, C., Frêne, C., 2010. Efecto de plantaciones de *Pinus radiata* y Eucalyptus globulus sobre el recurso agua en la Cordillera de la Costa de la región del Biobío, Chile. Bosque 31, 219–230.
Huxman, T.E., Cable, J.M., Ignace, D.D., Eilts, J.A., English, N.B., Weltzin, J., Williams, D.G., 2004. Response of net ecosystem gas exchange to a simulated precipitation pulse in a semi-arid grassland: the role of native versus non-native grasses and soil texture. Oecologia 141, 295–305.
Huxman, T.E., Wilcox, B., Breshears, D.D., Scott, R.L., Snyder, K., Small, E.E., Hultine, K., Pockman, W., Jackson, R.B., 2005. Ecohydrological implications of woody plant encroachment. Ecology 86, 308–319.
Iroumé, A., Huber, A., 2002. Comparison of interception losses in a broadleaved native forest and a *Pseudotsuga menziesii* (Douglas fir) plantation in the Andes Mountains of southern Chile. Hydrol. Process. 16, 2347–2361.
Iroumé, A., Mayen, O., Huber, A., 2006. Runoff and peak flow responses to timber harvest and forest age in southern Chile. Hydrol. Process. 20, 37–50.
Kurc, S.A., Small, E.E., 2004. Dynamics of evapotranspiration in semiarid grassland and shrubland ecosystems during the summer monsoon season, central New Mexico. Water Resour. Res. 40, 15.
Lara, A., Soto, D., Armesto, J., Donoso, P., Wernli, C., Nahuelhual, L., Squeo, F., 2003. Componentes científicos clave para una política nacional sobre usos, servicios y conservación de los bosques nativos Chilenos. Universidad Austral de Chile, Valdivia.
Lara, A., Little, C., Urrutia, R., McPhee, J., Álvarez-Garretón, C., Oyarzún, C., Soto, D., Donoso, P., Nahuelhual, L., Pino, M., Arismendi, I., 2009. Assessment of ecosystem services as an opportunity for the conservation and management of native forests in Chile. For. Ecol. Manage. 258, 415–424.
Liang, S., 2001. Narrowband to broadband conversions of land surface albedo I Algorithms. Remote Sens. Environ. 76, 213–238.
Little, C., Lara, A., McPhee, J., Urrutia, R., 2009. Revealing the impact of forest exotic plantations on water yield in large scale watersheds in south-central Chile. J. Hydrol. 374, 162–170.
Mattar, C., Franch, B., Sobrino, J.A., Corbari, C., Jiménez-Muñoz, J.C., Olivera-Guerra, L., Skokovic, D., Sória, G., Oltra-Carriò, R., Julien, Y., Mancini, M., 2013. Angular effects on actual evapotranspiration estimated by S-SEBI model over an agricultural area: Part 1, influences of the broad-band albedo. Remote Sensing of Environment.
Meza, F., Varas, E., 2000. Estimation of mean monthly solar global radiation as a function of temperature. Agric. For. Meteorol. 100, 231–241.
Moreira, M.Z., Martinelli, L.A., Victoria, R.L., Barbosa, E.M., Bonates, L.C.M., Nepstads, D.C., 1996. Contribution of transpiration to forest ambient vapour based on isotopic measurements. Global Change Biol. 3, 439–450.
Moussa, R., Chahinian, N., Bocquillon, C., 2007. Distributed hydrological modelling of a Mediterranean mountainous catchment – model construction and multi-site validation. J. Hydrol. 337, 35–51.
Mu, Q., Heinsch, F.A., Zhao, M., Running, S.W., 2007. Development of a global evapotranspiration algorithm based on MODIS and global meteorology data. Remote Sens. Environ. 106, 285–304.
Newman, B.D., Wilcox, B.P., Archer, S.R., Breshears, D.D., Dahm, C.N., Duffy, C.J., McDowell, N.G., Phillips, F.M., Scanlon, B.R., Vivoni, E.R., 2006. Ecohydrology of water-limited environments: a scientific vision. Water Resour. Res. 42, 1–15.
Ogawa, K., Schmugge, T., Jacob, F., 2003. Estimation of land surface window (8–12 μm) emissivity from multi-spectral thermal infrared remote sensing – a case study in a part of Sahara Desert. Geophys. Res. Lett. 30, 12–15.
Olivera, L., Mattar, C., Galleguillos, M., 2013. Estimación de la evapotranspiración real en ecosistemas mediterráneos de Chile mediante datos ASTER y MODIS. Rev. Teledetecc. 39, 46–56.
Paskoff, R., Manriquez, H., 1999. Ecosystem and legal framework for coastal management in central Chile. Ocean Coast. Manage. 42, 105–117.
Pizarro, R., Araya, S., Jordan, C., Farías, C., Flores, J.P., Bro, P.B., 2006. The effects of changes in vegetative cover on river flows in the Purapel river basin of central Chile. J. Hydrol. 327, 249–257.
Pôças, I., Cunha, M., Pereira, L.S., Allen, R.G., 2013. Using remote sensing energy balance and evapotranspiration to characterize montane landscape vegetation with focus on grass and pasture lands. Int. J. Appl. Earth Obs. Geoinf. 21, 159–172.
Roerink, G.J., Su, Z., Menenti, M., 2000. S-SEBI: a simple remote sensing algorithm to estimate the surface energy balance. Phys. Chem. Earth, Part B: Hydrol. Oceans Atmos. 25, 147–157.
Rouse, J.W., Haas, Jr. R.H., Schell, J.A., Deering, D.W. 1973. Monitoring the vernal advancement and retrogradation (green wave effect) of natural vegetation. Prog. Rep. RSC 1978-1, Remote Sensing Center, Texas A&M Univ., College Station, 93p. (NTIS No. E73-106393).
San Martín J., Donoso C., 1997. Estructura florística e impacto antrópico en el bosque Maulino de Chile. In: Armes- to JJ, Villagrán C., Arroyo M.K. (Eds.), Ecología de los bosques nativos de Chile. Editorial Universitaria, Santiago, Chile, pp. 153–168.
Sobrino, J.A., Gómez, M., Jiménez-Muñoz, J.C., Olioso, A., 2007. Application of a simple algorithm to estimate daily evapotranspiration from NOAA–AVHRR images for the Iberian Peninsula. Remote Sens. Environ. 110, 139–148.
Sobrino, J.A., Gómez, M., Jiménez-Muñoz, J.C., Olioso, A., Chehbouni, G., 2005. A simple algorithm to estimate evapotranspiration from DAIS data: application to the DAISEX campaigns. J. Hydrol. 315, 117–125.
Sobrino, J.A., Jiménez Muñoz, J.C., Sòria, G., Gómez, M., Ortiz, A.B., Romaguera, M., Zaragoza, M., Julien, Y., Cuenca, J., Atitar, M., Hidalgo, V., Franch, B., Mattar, C., Ruescas, A., Morales, L., Gillespie, A., Balick, L., Su, Z., Nerry, F., Peres, L., Libonati, R., 2008. Thermal remote sensing in the framework of the SEN2FLEX project: field measurements, airborne data and applications. Int. J. Remote Sens. 29, 4961–4991.
Soil Survey Division Staff, USDA. 1993. Soil Survey Manual. USDA, Handbook N°18. U.S. Government Printing Office, Washington, DC 20402, 437 p.
Taylor, J.A., Jacob, F., Galleguillos, M., Prévot, L., Guix, N., Lagacherie, P., 2013. The utility of remotely-sensed vegetative and terrain covariates at different spatial resolutions in modelling soil and watertable depth (for digital soil mapping). Geoderma 193–194, 83–93.
Tucker, C.J., 1979. Red and photographic infrared linear combinations for monitoring vegetation. Remote Sensing of Environment 8, 127–150.
Verstraeten, W.W., Veroustraete, F., Feyen, J., 2005. Estimating evapotranspiration of European forests from NOAA-imagery at satellite overpass time: towards an operational processing chain for integrated optical and thermal sensor data products. Remote Sens. Environ. 96, 256–276.
Wang, K., Wang, P., Li, Z., Cribb, M., Sparrow, M., 2007. A simple method to estimate actual evapotranspiration from a combination of net radiation, vegetation index, and temperature. J. Geophys. Res. 112, D15107.
Yang, F., White, M.A., Michaelis, A.R., Ichii, K., Hashimoto, H., Votava, P., Zhu, A., Nemani, R.R., 2006. Prediction of continental-scale evapotranspiration by combining MODIS and AmeriFlux data through support vector machine. IEEE Trans. Geosci. Remote Sens. 44, 3452–3461.
Yepez, E.A., Huxman, T.E., Ignace, D.D., English, N.B., Weltzin, J.F., Castellanos, A.E., Williams, D.G., 2005. Dynamics of transpiration and evaporation following a moisture pulse in semiarid grassland: a chamber-based isotope method for partitioning flux components. Agric. For. Meteorol. 132, 359–376.
Zhang, L., Dawes, W.R., Walker, G.R., 2001. Response of mean annual evapotranspiration to vegetation changes at catchment scale. Water Resour. Res. 37, 701–708.
Zhao, M., Heinsch, F.A., Nemani, R.R., Running, S.W., 2005. Improvements of the MODIS terrestrial gross and net primary production global data set. Remote Sens. Environ. 95, 164–176.